Performance Analysis of RIS-Assisted Wireless Communications with Energy Harvesting

Bingxin Zhang, *Student Member, IEEE*, Kun Yang, *Senior Member, IEEE*, Kezhi Wang, *Senior Member, IEEE*, and Guopeng Zhang

***Abstract*—In this paper, we investigate a reconfigurable intelligent surface (RIS)-assisted wireless communication system with energy harvesting. In the single information user (IU) scenario, we consider the power control of base station (BS) and the random deployment of energy users (EUs). To this end, we first characterize the statistical features of the channel gains over BS-RIS-IU and BS-RIS-EU cascaded links. Then, we derive a closed-form expression of the information outage probability (IOP) of the IU and show an upper bound of the energy outage probability (EOP) of EUs by invoking the Jensen's inequality. Furthermore, we consider two more general extensions, namely, the existence of imperfect phase alignment and multiple IUs. Finally, the correctness of the analysis results is verified by Monte-Carlo simulation.**

***Index Terms*—Reconfigurable intelligent surface, energy harvesting, outage probability, stochastic geometry.**

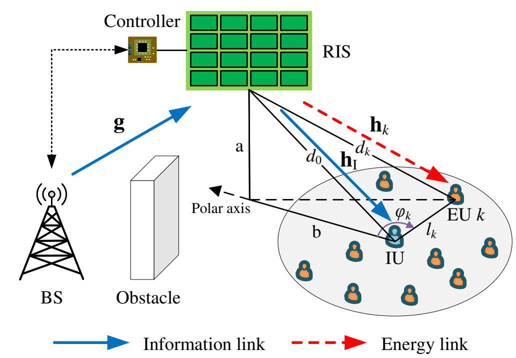

Fig. 1. The system model.

I. Introduction

Reconfigurable intelligent surface (RIS) has drawn significant attention due to its superior capability in reconfiguring the wireless propagation environment [1], [2]. Specifically, the RIS consists of a large number of low-cost passive reflecting elements, each of which can be independently controlled via the superposition or subtraction of its reflected signals to increase the desired signal power or suppress co-channel interference, thus improving the performance of wireless systems [3], [4].

Many works have studied the performance of RIS-assisted wireless communications. In [5], the authors considered a RIS-aided wireless system with imperfect channel state information (CSI), and derived the closed-form expressions of the outage probability, average bit error rate, and average capacity. The authors in [6] analyzed the performance of RIS-assisted wireless communication systems affected by outdated CSI. In [7], the authors investigated an RIS-assisted heterogeneous network under channel uncertainties and residual hardware impairments. The authors in [8] characterized the spatial throughput of a multiple RIS-assisted single-cell multi-user system, in which RISs and users are randomly distributed in a two-dimensional space. The authors in [9] considered a RIS-empowered multi-user multiple-input single-output uplink communication system and proposed a parallel factor decomposition based channel estimation framework. In [10], the authors studied the random rotations scheme at the RIS, in which the reflecting elements do not need any CSI and only use random phase rotations. However, none of the above works utilized radio frequency (RF) resources to improve users' energy sustainability.

As a solution to prolong the lifetime of energy-constrained Internet of Things devices, RF energy harvesting techniques have been intensively studied and applied in practical applications [11]. The authors in [12] studied the performance of a RIS-assisted simultaneous wireless information and power transfer (SWIPT) system for quantized phase shifts at the RIS. In [13], the authors aimed at maximizing the weighted sum rate of all information receivers by jointly optimizing the transmit beamforming of the base station (BS) and the phase shifts for a RIS-assisted SWIPT multiple-input multiple-output system. The authors in [14] maximized the total energy efficiency of all wireless devices in a RIS-assisted wireless-powered communication network by jointly optimizing radio resources and passive beamforming. Nevertheless, previous works ignore that energy harvesting devices are normally randomly deployed in practical scenarios.

Against the above background, this paper considers a RIS-

(Corresponding author: Kun Yang.)

Bingxin Zhang is with the School of Information and Communication Engineering, University of Electronic Science and Technology of China, Chengdu 611731, China (e-mail: bxzhang@std.uestc.edu.cn).

Kun Yang is with the School of Information and Communication Engineering, University of Electronic Science and Technology of China, Chengdu 611731, China, and also with the School of Computer Science and Electronic Engineering, University of Essex, Colchester CO4 3SQ, U.K. (e-mail: kunyang@essex.ac.uk).

Kezhi Wang is with the Department of Computer and Information Sciences, Northumbria University, Newcastle upon Tyne NE1 8ST, U.K. (e-mail: kezhi.wang@northumbria.ac.uk).

Guopeng Zhang is with the School of Computer Science and Technology, China University of Mining and Technology, Xuzhou 221116, China (e-mail: gpzhang@cumt.edu.cn).

The authors would like to thank the financial support of National Natural Science Foundation of China (No. 62132004, 61971421), Sichuan Major R&D Project (No. 22QYCX0168) and EU H2020 Project COSAFE (GA-824019).

assisted wireless communication with energy harvesting abilities. Different from the prior works, we assume that all energy users (EUs) are randomly deployed in a disc centered at an information user (IU). Moreover, we consider that the BS has the ability of power control. Specifically, the main contributions of our work are summarized as follows:

- According to the statistical characteristics of channel gains, we derive a closed-form expression of the information outage probability (IOP) of the IU under a given rate threshold.
- By using a binomial expansion function, we obtain the expectation of the distance from EUs to the RIS in the closed-form. Then, we present an upper bound of the energy outage probability (EOP) of EUs under a given energy threshold by invoking Jensen's inequality.
- Furthermore, we study the performance in the existence of imperfect phase alignment. We also analyze the system performance with multiple IUs scenarios.

II. System Model and Statistical Features

We consider a RIS-assisted wireless system with energy harvesting abilities, as depicted in Fig. 1. The system consists of a BS, an IU, K ($K \geq 1$) EUs and a RIS with N reflecting elements. The BS and all users are equipped with a single antenna. In this scenario, the BS sends information to the IU, while K EUs harvest energy from the RF signals. For tractability purposes, we assume that K EUs are uniformly and randomly distributed in a circle, centered at the IU, with radius L meters (m).

As shown in Fig. 1, by using the polar coordinate system with the location of the IU as the reference point, the k-th EUs' position is defined by (l_k, ψ_k), where l_k and ψ_k are the radial and angular coordinates, respectively, $\forall k \in \{1, ..., K\}$. Considering the random deployment of EUs, the corresponding probability density function (PDF) of the angular coordinate can be expressed as [15]

$$f_{\psi_k}(\psi_k) = \frac{1}{2\pi}, \psi_k \in [0, 2\pi]. \tag{1}$$

For the radial coordinate, its PDF can be obtained by differentiating the cumulative distribution function (CDF) over the radial variable l_k, thus the PDF of $l_k \in [0, L]$ can be shown as [15]

$$f_{l_k}(l_k) = \frac{\mathrm{d}F_{l_k}(l_k)}{\mathrm{d}l_k} = \frac{2l_k}{L^2}, l_k \in [0, L]. \tag{2}$$

Furthermore, let a denote the vertical height of the RIS, b denote the distance from the IU to the projection point of the RIS at the users' plane, d_{SR} denote the distance from the BS to the RIS, d_0 and d_k denote the distances from the RIS to the IU and the k-th EU, respectively. Therefore, one can have $d_0 = \sqrt{a^2 + b^2}$. For calculation of d_k, the law of cosines can be exploited, thus one has [16]

$$d_k = \sqrt{a^2 + b^2 + l_k^2 - 2bl_k \cos\psi_k}. \tag{3}$$

We assume that the links between the BS and all users can only be established through the RIS, where the direct links may be weak or blocked due to severe blockage. The complex channel vectors from the BS to the RIS, from the RIS to the IU and the k-th EU are denoted by $\mathbf{g} \in \mathbb{C}^{N\times 1}$, $\mathbf{h}_{\mathrm{I}} \in \mathbb{C}^{N\times 1}$ and $\mathbf{h}_k \in \mathbb{C}^{N\times 1}$, respectively. In this paper, we assume a block-fading channel which consists of distance-dependent path-loss and a small-scale fading [17]. Therefore, these channels are modeled as $[\mathbf{g}]_n = g_n d_{\mathrm{SR}}^{-\frac{\alpha}{2}}$, $[\mathbf{h}_{\mathrm{I}}]_n = h_{\mathrm{I},n} d_0^{-\frac{\alpha}{2}}$ and $[\mathbf{h}_k]_n = h_{k,n} d_k^{-\frac{\alpha}{2}}$, where g_n, $h_{\mathrm{I},n}$, $h_{k,n} \sim \mathcal{CN}(0,1)$ denote the small-scale Rayleigh fading, respectively, $\forall n \in \{1, ..., N\}$, $k \in \{1, ..., K\}$, and α is the path-loss exponent. Then, the received signal at the IU can be written as

$$y_{\mathrm{I}} = \sqrt{P_t}\mathbf{g}^{\mathrm{T}}\mathbf{\Phi}\mathbf{h}_{\mathrm{I}} x_{\mathrm{I}} + w_{\mathrm{I}}, \tag{4}$$

where x_{I} is the information symbol with $\mathbb{E}\{||x_{\mathrm{I}}||^2\} = 1$, P_t is the transmit power, $w_{\mathrm{I}} \sim \mathcal{CN}(0, \sigma^2)$ is the additive white Gaussian noise at the IU, and $\mathbf{\Phi} = \mathrm{diag}(e^{j\phi_1}, ..., e^{j\phi_N})$ is the diagonal coefficient matrix with the phase shift of the n-th reflecting element $\phi_n \in [0, 2\pi)$. Then, the instantaneous signal-to-noise ratio (SNR) at the IU is given by

$$\gamma = \frac{P_t}{\sigma^2}\left|\sum_{n=1}^{N}[\mathbf{g}]_n[\mathbf{h}_{\mathrm{I}}]_n e^{j\phi_n}\right|^2 = \frac{P_t}{\sigma^2} d_{\mathrm{SR}}^{-\alpha} d_0^{-\alpha}\left|\sum_{n=1}^{N} g_n h_{\mathrm{I},n} e^{j\phi_n}\right|^2. \tag{5}$$

We assume that the channel state information (CSI) of the BS-RIS and RIS-IU links can be obtained at the BS. Therefore, to maximize the received SNR, the RIS should carefully adjust the phase shift coefficients to satisfy $\phi_n = -\arg(g_n) - \arg(h_{\mathrm{I},n})$, $\forall n \in \{1, ..., N\}$. As a result, γ can be rewritten as

$$\gamma = \frac{P_t}{\sigma^2} d_{\mathrm{SR}}^{-\alpha} d_0^{-\alpha}\left(\sum_{n=1}^{N}|g_n|\,|h_{\mathrm{I},n}|\right)^2. \tag{6}$$

Then, the achievable rate R (bit/s/Hz) of the IU can be expressed as follows

$$R = \log_2(1 + \gamma). \tag{7}$$

Since EUs are not currently scheduled users, we assume that the CSI from the RIS to EUs is unavailable. As a result, the harvested energy at the k-th EU can be written as

$$E_k = \eta\tau P_t d_{\mathrm{SR}}^{-\alpha} d_k^{-\alpha}\left|\sum_{n=1}^{N} g_n h_{k,n} e^{j\phi_n}\right|^2, \tag{8}$$

where $0 < \eta < 1$ is the energy conversion efficiency of EUs and τ is the duration of energy harvesting.

We also consider that the BS has the ability of power control. In other words, given a rate threshold R_{th} of the IU, the BS can adjust its transmit power to an optimal value. Therefore, based on (6) and (7), the optimal power of the BS can be given by

$$P_t^* = \frac{\left(2^{R_{\mathrm{th}}} - 1\right)\sigma^2}{d_{\mathrm{SR}}^{-\alpha} d_0^{-\alpha}\left(\sum_{n=1}^{N}|g_n|\,|h_{\mathrm{I},n}|\right)^2}. \tag{9}$$

Then, substituting (9) into (8), the harvested energy of the k-th UE can be rewritten as

$$E_k = \frac{\eta\tau\rho\sigma^2 d_k^{-\alpha}\left|\sum_{n=1}^{N} g_n h_{k,n} e^{j\phi_n}\right|^2}{d_0^{-\alpha}\left(\sum_{n=1}^{N}|g_n|\,|h_{\mathrm{I},n}|\right)^2}, \tag{10}$$

where $\rho = 2^{R_{\mathrm{th}}} - 1$.

III. Performance Analysis

In this section, we first identify the channel statistical characteristics of the IU and EUs. Then, we derive the IOP of the IU and the EOP of EUs under the given threshold.

A. Channel Gain Characterization

Define $X = \left(\sum_{n=1}^{N} |g_n| \, |h_{\mathrm{I},n}|\right)^2$, and we first identify the statistical characteristics of X. However, it is difficult to derive the exact distribution of X. To tackle this difficulty, we employ the moment matching technique to approximate X by Gamma distribution [18]. The first and second moments of the random variable X are denoted by $u_X = \mathbb{E}\{X\}$ and $v_X = \mathbb{E}\{X^2\}$, respectively. As a result, the CDF and PDF of X can be respectively expressed as

$$F_X(x) = \frac{1}{\Gamma(\beta)} \Upsilon\left(\beta, \frac{x}{\theta}\right), \tag{11}$$

$$f_X(x) = \frac{1}{\Gamma(\beta)\theta^{\beta}} x^{\beta-1} e^{-\frac{x}{\theta}}, \tag{12}$$

where $\beta = \frac{u_X^2}{v_X - u_X^2}$, $\theta = \frac{v_X - u_X^2}{u_X}$, $\Gamma(\cdot)$ represents the Gamma function and $\Upsilon(\cdot,\cdot)$ denotes the lower incomplete Gamma function. In particular, u_X and v_X are given in [18, Eq. (A5)].

Let $Y_k = \left|\sum_{n=1}^{N} g_n h_{k,n} e^{j\phi_n}\right|^2$. Similar to [19], Y_k can be approximated as an exponential random variable with mean $\lambda_k = N$. As a result, the CDF of Y_k can be written as

$$F_{Y_k}(y) = 1 - e^{-\frac{y}{\lambda_k}}. \tag{13}$$

B. The IOP of the IU and the EOP of EUs

In this subsection, the IOP of the IU and the EOP of EUs under a given threshold are derived.

Lemma 1. Given a rate threshold R_{th}, the IOP of the IU is given by

$$P_{\mathrm{I}}^{\mathrm{O}} = \frac{1}{\Gamma(\beta)} \Upsilon\left(\beta, \frac{\rho\sigma^2}{\theta d_{\mathrm{SR}}^{-\alpha} d_0^{-\alpha} P_{\mathrm{th}}}\right), \tag{14}$$

where P_{th} denotes the maximum transmit power of the BS.

Proof: Based on (6), (7) and (9), one has

$$\begin{aligned} P_{\mathrm{I}}^{\mathrm{O}} &= \Pr\{R < R_{\mathrm{th}}\} = \Pr\left\{\frac{P_t^*}{\sigma^2} d_{\mathrm{SR}}^{-\alpha} d_0^{-\alpha} X < \rho\right\} \\ &\overset{(a)}{=} \Pr\left\{\frac{P_{\mathrm{th}}}{\sigma^2} d_{\mathrm{SR}}^{-\alpha} d_0^{-\alpha} X < \rho\right\} = \Pr\left\{X < \frac{\rho\sigma^2}{d_{\mathrm{SR}}^{-\alpha} d_0^{-\alpha} P_{\mathrm{th}}}\right\} \\ &= F_X\left(\frac{\rho\sigma^2}{d_{\mathrm{SR}}^{-\alpha} d_0^{-\alpha} P_{\mathrm{th}}}\right), \end{aligned} \tag{15}$$

where (a) follows the case that the outage event for the IU only occurs when $P_t^* > P_{\mathrm{th}}$.

Then, by substituting (11) into (15), one can obtain (14) after some mathematical manipulations. ■

Furthermore, given a energy threshold E_{th}, the EOP of the k-th EU can be expressed as

$$\begin{aligned} P_{\mathrm{E}_k}^{\mathrm{O}} &= \Pr\{E_k < E_{\mathrm{th}}\} = \Pr\left\{\frac{\eta\tau\rho\sigma^2 d_k^{-\alpha} Y_k}{d_0^{-\alpha} X} < E_{\mathrm{th}}\right\} \\ &= \Pr\left\{Y_k < \frac{X d_0^{-\alpha} E_{\mathrm{th}}}{\eta\tau\rho\sigma^2 d_k^{-\alpha}}\right\} = \Pr\left\{\frac{Y_k}{X} < \Omega d_k^{\alpha}\right\}, \end{aligned} \tag{16}$$

where $\Omega = \frac{E_{\mathrm{th}} d_0^{-\alpha}}{\eta\tau\rho\sigma^2}$.

Note that the closed-form expression of (16) is difficult to obtain directly. To this end, let $Z = \frac{Y_k}{X}$, and we first apply the following lemma to show the statistical features of Z.

Lemma 2. The CDF of Z can be obtained as

$$F_Z(z) = 1 - \frac{\lambda_k^{\beta}}{(\theta z + \lambda_k)^{\beta}}, \tag{17}$$

Proof: Based on (12) and (13), one has

$$\begin{aligned} F_Z(z) &= \Pr\{Z < z\} = \Pr\{Y_k < Xz\} \\ &= \int_0^{\infty} F_{Y_k}(zt) f_X(t) \mathrm{d}t \\ &= \frac{1}{\Gamma(\beta)\theta^{\beta}} \int_0^{\infty} \left(1 - e^{-\frac{zt}{\lambda_k}}\right) t^{\beta-1} e^{-\frac{t}{\theta}} \mathrm{d}t \\ &= \frac{1}{\Gamma(\beta)\theta^{\beta}} \left(\int_0^{\infty} t^{\beta-1} e^{-\frac{t}{\theta}} \mathrm{d}t - \int_0^{\infty} t^{\beta-1} e^{-\frac{zt}{\lambda_k} - \frac{t}{\theta}} \mathrm{d}t\right) \\ &\overset{(a)}{=} 1 - \frac{1}{\theta^{\beta}\left(\frac{z}{\lambda_k} + \frac{1}{\theta}\right)^{\beta}}, \end{aligned} \tag{18}$$

where (a) follows [20, Eq. (3.381.4)]. Then, by operating some mathematical operations on (18), one can obtain (17). Hence, the proof is completed. ■

Considering the randomness of the location of EUs, the EOP of EUs shall be evaluated in the form of expectation, with respect to the polar coordinate consisting of radial and angular variable. Therefore, based on (3) and (17), (16) can be rewritten as

$$\begin{aligned} P_{\mathrm{E}_k}^{\mathrm{O}} &= \mathbb{E}_{d_k^{\alpha}}\left\{F_Z(\Omega d_k^{\alpha})\right\} \\ &= \mathbb{E}_{l_k,\psi_k}\left\{F_Z\left(\Omega\left(a^2 + b^2 + l_k^2 - 2bl_k\cos\psi_k\right)^{\frac{\alpha}{2}}\right)\right\}. \end{aligned} \tag{19}$$

However, it is difficult, if not impossible, to obtain the exact closed-form expression for $P_{\mathrm{E}_k}^{\mathrm{O}}$ in (19). To this end, we resort to an upper bound of (19) by invoking the Jensen's inequality as

$$P_{\mathrm{E}_k}^{\mathrm{O}} = \mathbb{E}_{d_k^{\alpha}}\left\{F_Z(\Omega d_k^{\alpha})\right\} \le F_Z\left(\Omega\mathbb{E}\left\{d_k^{\alpha}\right\}\right). \tag{20}$$

Next, we first derive the closed-form expression of $\mathbb{E}\{d_k^{\alpha}\}$ in (20).

Lemma 3. $\mathbb{E}\{d_k^{\alpha}\}$ in (20) can be expressed as

$$\mathbb{E}\left\{d_k^{\alpha}\right\} = \frac{1}{\pi L^2} \sum_{p=0}^{\frac{\alpha}{2}} \begin{pmatrix} \frac{\alpha}{2} \\ p \end{pmatrix} \Xi_{l_k} \Xi_{\psi_k}, \tag{21}$$

where

$$\Xi_{l_k} = \sum_{q=0}^{p} \begin{pmatrix} p \\ q \end{pmatrix} \frac{(-2b)^{\frac{\alpha}{2}-p}(a^2+b^2)^{p-q}}{\frac{\alpha}{2} - p + 2q + 2} L^{\frac{\alpha}{2}-p+2q+2}, \tag{22}$$

and

$$\Xi_{\psi_k} = 2^{\frac{\alpha}{2}-p}\left(1 + (-1)^{\frac{\alpha}{2}-p}\right) B\left(\frac{\frac{\alpha}{2} - p + 1}{2}, \frac{\frac{\alpha}{2} - p + 1}{2}\right), \tag{23}$$

with $B(\cdot,\cdot)$ being the beta function.

Proof: Based on (1) and (2), one has

$$\begin{aligned}\mathbb{E}\left\{d_k^\alpha\right\} &= \mathbb{E}_{l_k,\psi_k}\left\{\left(a^2+b^2+l_k^2-2bl_k\cos\psi_k\right)^{\frac{\alpha}{2}}\right\}\\ &= \int_0^L\int_0^{2\pi}\left(a^2+b^2+l_k^2-2bl_k\cos\psi_k\right)^{\frac{\alpha}{2}}\\ &\qquad\times f_{l_k}(l_k)f_{\psi_k}(\psi_k)\ \mathrm{d}l_k\mathrm{d}\psi_k\\ &= \frac{1}{\pi L^2}\int_0^L\int_0^{2\pi}\left(a^2+b^2+l_k^2-2bl_k\cos\psi_k\right)^{\frac{\alpha}{2}}\\ &\qquad\times l_k\ \mathrm{d}l_k\mathrm{d}\psi_k.\end{aligned} \tag{24}$$

Due to the independent radial and angle variables in users' polar coordinates, the radial-based and angle-based integrals in (24) can be combined by using a binomial expansion function. As a result, (24) can be rewritten as (21), in which Ξ_{l_k} and Ξ_{ψ_k} are the expectation operation with respect to the radial and angular in (24), respectively. Specifically,

$$\Xi_{l_k} = \int_0^L l_k\left(a^2+b^2+l^2\right)^p\left(-2bl_k\right)^{\frac{\alpha}{2}-p}\mathrm{d}l_k, \tag{25}$$

$$\Xi_{\psi_k} = \int_0^{2\pi}\left(\cos\psi_k\right)^{\frac{\alpha}{2}-p}\mathrm{d}\psi_k. \tag{26}$$

Furthermore, by using the binomial expansion to facilitate the corresponding integrals' calculation in (25) and (26), one can obtain (22) and (23) in the closed-form, respectively. Then, (21) can also be expressed in a closed-form. ■

Finally, substituting (17) and (21) into (20), one can obtain the upper bound of $P_{\mathrm{E}_k}^{\mathrm{O}}$ in a closed-form as follows

$$\overline{P_{\mathrm{E}_k}^{\mathrm{O}}} = 1-\frac{\lambda_k^\beta}{\left(\theta\Lambda+\lambda_k\right)^\beta}, \tag{27}$$

where $\Lambda = \frac{\Omega}{\pi L^2}\sum_{p=0}^{\frac{\alpha}{2}}\begin{pmatrix}\frac{\alpha}{2}\\ p\end{pmatrix}\Xi_{l_k}\Xi_{\psi_k}$.

Remark 1: For (27), given a specific path-loss exponent α and then simplified, we find that the EOP increases monotonically with L. Due to space limitations, the details of the proof are omitted.

IV. Extensions

In this section, we consider two more general extensions, namely, the existence of imperfect phase alignment and multiple IUs.

A. The existence of imperfect phase alignment

In this subsection, we investigate the case that the phase shift cannot be perfectly aligned, which may be caused by the imperfect CSI or limited quantization bits of the phase shifts of the RIS. Therefore, the SNR γ in (6) can be rewritten as

$$\gamma = \frac{P_t}{\sigma^2}d_{\mathrm{SR}}^{-\alpha}d_0^{-\alpha}\left|\sum_{n=1}^N|g_n||h_{\mathrm{I},n}|e^{j\varphi_n}\right|^2, \tag{28}$$

where φ_n is the error caused by imperfect phase alignment of the k-th element of the RIS. We consider that φ_n follows the uniform distribution, i.e., $\varphi_n\sim U(-\xi,\xi)$, and ξ characterizes the degree of the phase error [18]. When $\xi=0$, it reduces to the perfect CSI case in Section III.

Define $Q=\left|\sum_{n=1}^N|g_n||h_{\mathrm{I},n}|e^{j\varphi_n}\right|^2$, and we can approximate Q by a Gamma distribution, i.e. $Q\sim\mathrm{Gamma}(\beta',\theta')$, where the parameters β' and θ' are given in [18, Eq. (27)]. Then, the IOP of the IU in the case of imperfect phase alignment can be obtained by using the same method in Subsection III-B. In particular, since we have assumed that the CSI from the RIS to EUs is not available, the performance of EUs is not affected by imperfect phase alignment.

B. The existence of multiple IUs

In this subsection, we consider that the BS broadcasts information to M IUs. Similar to EUs, the IUs are also uniformly and randomly distributed in the circle centered on the 0-th IU. For tractability of the analysis, we consider that the RIS employs equal phase shifts, i.e. $\phi_n^{'}=\phi_i^{'}$, $\forall n,i\in\{1,...,N\}$. Therefore, the SNR at the m-th IU can be expressed as

$$\gamma_m = \frac{P_t}{\sigma^2}d_{\mathrm{SR}}^{-\alpha}d_m^{-\alpha}\left|\sum_{n=1}^N g_nh_{m,n}e^{j\phi_n^{'}}\right|^2, \tag{29}$$

where d_m is the distance between the RIS and the m-th IU and $h_{m,n}$ denotes the complex channel coefficient from the n-th element of the RIS to the m-th IU, $\forall m\in\{0,1,...,M-1\}$.

Next, define $F=\left|\sum_{n=1}^N g_nh_{m,n}e^{j\phi_n^{'}}\right|^2$. We first identify the statistical characteristics of F.

Lemma 4. The first and second moments of F are given by

$$u_F = N \quad \text{and} \quad v_F = 2N(N+1), \tag{30}$$

respectively.

Proof: In this case, the first moment of F can be written as

$$\begin{aligned}u_F = \mathbb{E}\{F\} &= \mathbb{E}\left\{\left(\sum_{n=1}^N g_nh_{m,n}e^{j\phi_n^{'}}\right)\left(\sum_{n=1}^N g_nh_{m,n}e^{j\phi_n^{'}}\right)\right\}\\ &= \mathbb{E}\left\{\sum_{n=1}^N|g_n|^2|h_{m,n}|^2\right\}+\mathbb{E}\left\{\sum_{i\neq n}g_ih_{m,i}g_n^*h_{m,n}^*\right\}.\end{aligned} \tag{31}$$

Since $|g_n|$ and $|h_{m,n}|$ follow Rayleigh distribution, one has $\mathbb{E}\left\{|g_n|^2\right\}=\mathbb{E}\left\{|h_{m,n}|^2\right\}=1$. Therefore, the first term of (31) is given by

$$\mathbb{E}\left\{\sum_{n=1}^N|g_n|^2|h_{m,n}|^2\right\} = \sum_{n=1}^N\mathbb{E}\left\{|g_n|^2|h_{m,n}|^2\right\} = N. \tag{32}$$

Since g_i and $h_{m,i}$ are assumed to be uncorrelated with g_n^* and $h_{m,n}^*$, respectively, one has $\mathbb{E}\left\{g_ig_n^*\right\}=\mathbb{E}\left\{h_{m,i}h_{m,n}^*\right\}=0$. As a result, one has

$$\mathbb{E}\left\{\sum_{i\neq n}g_ih_{m,i}g_n^*h_{m,n}^*\right\} = \sum_{i\neq n}\mathbb{E}\left\{g_ig_n^*\right\}\mathbb{E}\left\{h_{m,i}h_{m,n}^*\right\} = 0. \tag{33}$$

Then, substituting (32) and (33) into (31) yields u_F in (30). The second moment of F is given by

$$v_F = \mathbb{E}\left\{F^2\right\} = \mathbb{E}\left\{\left(\sum_{n=1}^{N}|g_n|^2|h_{m,n}|^2 + \sum_{i\neq n} g_i h_{m,i} g_n^* h_{m,n}^*\right)^2\right\}. \tag{34}$$

Then, define $J_1 = \sum_{n=1}^{N}|g_n|^2|h_{m,n}|^2$, $J_2 = \sum_{i\neq n} g_i h_{m,i} g_n^* h_{m,n}^*$, and (34) can be rewritten as

$$v_F = \mathbb{E}\left\{{J_1}^2\right\} + \mathbb{E}\left\{2J_1J_2\right\} + \mathbb{E}\left\{{J_2}^2\right\}. \tag{35}$$

For the first term in (35), one has

$$\begin{aligned}\mathbb{E}\left\{{J_1}^2\right\} &= \mathbb{E}\left\{\sum_{n=1}^{N}|g_n|^4|h_{m,n}|^4\right\} \\ &+ \mathbb{E}\left\{\sum_{i\neq n}|g_n|^2|h_{m,n}|^2|g_i|^2|h_{m,i}|^2\right\} \\ &= 4N + N(N-1),\end{aligned} \tag{36}$$

where

$$\mathbb{E}\left\{\sum_{n=1}^{N}|g_n|^4|h_{m,n}|^4\right\} = \sum_{n=1}^{N}\mathbb{E}\left\{|g_n|^4|h_{m,n}|^4\right\} = 4N \tag{37}$$

due to $\mathbb{E}\left\{|g_n|^4\right\} = \mathbb{E}\left\{|h_{m,n}|^4\right\} = 2$, and

$$\mathbb{E}\left\{\sum_{i\neq n}|g_n|^2|h_{m,n}|^2|g_i|^2|h_{m,i}|^2\right\} = N(N-1) \tag{38}$$

by using Isserlis' theorem [21] and $\mathbb{E}\left\{|g_n|^2|h_{m,n}|^2\right\} = 1$.

For the second term in (35), one has $\mathbb{E}\left\{2J_1J_2\right\} = 0$ by using (33). Moreover, for the third term in (35), one has

$$\begin{aligned}\mathbb{E}\left\{{J_2}^2\right\} &= \mathbb{E}\left\{\sum_{i\neq n, p\neq q} g_i h_{m,i} g_n^* h_{m,n}^* g_p h_{m,p} g_q^* h_{m,q}^*\right\} \\ &\overset{(a)}{=}\mathbb{E}\left\{\sum_{i\neq n}|g_i|^2|h_{m,i}|^2|g_n|^2|h_{m,n}|^2\right\} \overset{(d)}{=} N(N-1),\end{aligned} \tag{39}$$

where (a) is due to the existence of non-zero values only if $i = q$ and $n = p$, and step (d) follows (38). Finally, substituting (36) and (39) into (35), one can obtain v_F in (30). ■

Based on (30), F can be approximated as the Gamma distribution $F \sim \text{Gamma}(\beta'', \theta'')$, where $\beta'' = \frac{u_F^2}{v_F - u_F^2}$ and $\theta'' = \frac{v_F - u_F^2}{u_F}$.

On the other hand, the harvested energy at the k-th EU is given by

$$E_k = \eta\tau P_t d_{\text{SR}}^{-\alpha} d_k^{-\alpha}\left|\sum_{n=1}^{N} g_n h_{k,n} e^{j\phi_n'}\right|^2. \tag{40}$$

Define $W = \left|\sum_{n=1}^{N} g_n h_{k,n} e^{j\phi_n'}\right|^2$. Similar to the variable F, W can also be approximated by a Gamma distribution. Then, the IOP of IUs and the EOP of EUs can be obtained by using the same method in Subsection III-B.

V. Numerical Results and Discussions

In this section, Monte-Carlo simulations are conducted to validate our analytical results. Unless otherwise specified, the simulation parameters are set as follows: $\eta = 0.95$ [22], $\sigma^2 = -64$ dBm [23], $R_{\text{th}} = 10$ bit/s/Hz [24], $\alpha = 2$, $\tau = 1$ s, $a = 5$ m, $b = 10$ m and $d_{\text{SR}} = 10$ m. The curves labelled 'Simulation' are obtained by averaging over 10^6 random samples.

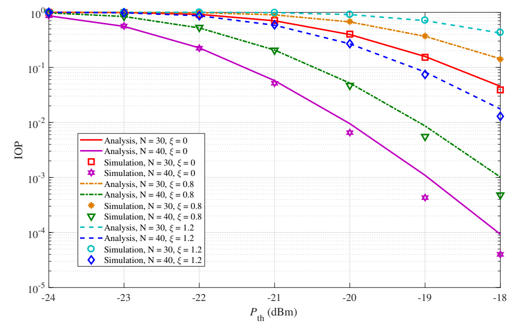

Fig. 2. P_{th} of the BS versus the IOP of the IU with $R_{\text{th}} = 10$ bit/s/Hz.

Fig. 2 depicts the IOP versus P_{th}, with $N \in \{30, 40\}$ and $\xi \in \{0, 0.8, 1.2\}$. One can see that our 'Analysis' curves match well with the simulation results, showing the accuracy and the usefulness of the derived expression. It is observed that the IOP decreases with the increase of P_{th}, showing an improvement in the system performance. This is because with the increase of P_{th}, the BS can support higher information transmission rate. Also, for the same P_{th}, larger value of N leads to better IOP performance. In addition, larger phase alignment error yields higher IOP, meaning that high-precision phase shifts are not negligible for improving the system performance.

Fig. 3 shows the EOP versus L, with $N \in \{10, 50\}$ and $\xi \in \{0, 0.8, 1.2\}$. The corresponding 'Analysis' curves are plotted by using (27). One can see that the EOP monotonically increases with L, as expected. This is because with the increase of L, the transmitted signals experience long distance from the RIS to UEs, namely, they suffer a larger path-loss, resulting in less harvested energy. In particular, by numerical simulations, we find that the product of θ and Λ in (27) is a small number compared to λ_k, and grows slowly with L. As a result, one can see that the curves in the figure are flat. It is also observed that for any given L, the EOP increases with the number of reflecting elements. The reason is that the cascaded BS-RIS-IU links can obtain N^2 order power gain [18], i.e. $X \sim \mathcal{O}(N^2)$, while the BS-RIS-EU links can only obtain N order power gain [19], i.e. $Y_k \sim \mathcal{O}(N)$. As a result, it can be seen from (10) that the harvested energy by EUs decreases with the increase of N. In addition, larger phase alignment error leads to a lower EOP. This is because that higher phase alignment error forces the BS to increase the transmit power, which increases the energy harvested by EUs.

In Fig. 4, the performance in the existence of multiple IUs is illustrated for $N \in \{20, 70, 120\}$. As shown in Fig. 4(a) and Fig. 4(c), the IOP and EOP decrease with the increase of P_t, respectively. This means that enhancing the transmit power of the BS can improve the performance of both IUs

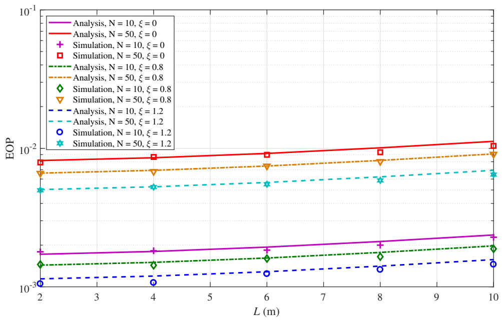

Fig. 3. L versus the EOP of the k-th EU with $R_{\rm th} = 10$ bit/s/Hz.

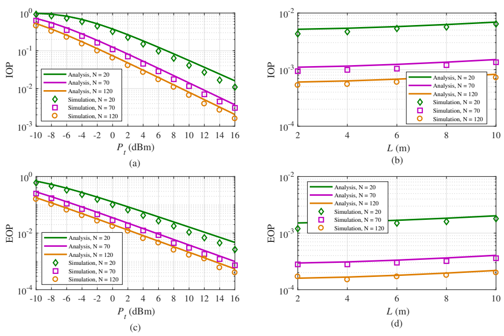

Fig. 4. Performance analysis in the existence of multiple IUs.

and EUs. In Fig. 4(b) and Fig. 4(d), one can see that the IOP and EOP monotonically increase with L, as expected. In particular, the interval between the curves in each subgraph of Fig. 4 decreases with the increase of N.

VI. Conclusion

In this paper, we have studied the performance of the RIS-assisted wireless communication system with energy harvesting over Rayleigh fading channels and random EU locations. In the single IU scenario, we obtain the closed-form expressions of the IOP and EOP by considering the power control of the BS. One sees that with the increase of reflecting element of the RIS, the IOP drops while the EOP improves. In addition, we evaluate the performance in the existence of imperfect phase alignment. We also analyze the system performance with multiple IUs. Numerical results have been carried out to verify the effectiveness of the derived expressions. For future work, we aim to further analyze the overall performance and the power allocation strategy of the system where the BS and user have multiple antennas.

References

[1] Q. Wu and R. Zhang, "Towards smart and reconfigurable environment: Intelligent reflecting surface aided wireless network," *IEEE Communications Magazine*, vol. 58, no. 1, pp. 106–112, 2020.

[2] A. Bhowal and S. Aissa, "RIS-aided communications in indoor and outdoor environments: Performance analysis with a realistic channel model," *IEEE Transactions on Vehicular Technology*, early access, Jan. 20, 2022, doi : 10.1109/TVT.2022.3143841.

[3] P. Xu, W. Niu, G. Chen, Y. Li, and Y. Li, "Performance analysis of RIS-assisted systems with statistical channel state information," *IEEE Transactions on Vehicular Technology*, vol. 71, no. 1, pp. 1089–1094, 2022.

[4] C. Huang, S. Hu, G. C. Alexandropoulos, A. Zappone, C. Yuen, R. Zhang, M. D. Renzo, and M. Debbah, "Holographic MIMO surfaces for 6G wireless networks: Opportunities, challenges, and trends," *IEEE Wireless Communications*, vol. 27, no. 5, pp. 118–125, 2020.

[5] P. Yang, L. Yang, and S. Wang, "Performance analysis for RIS-aided wireless systems with imperfect CSI," *IEEE Wireless Communications Letters*, vol. 11, no. 3, pp. 588–592, 2022.

[6] Y. Zhang, J. Zhang, M. Di Renzo, H. Xiao, and B. Ai, "Reconfigurable intelligent surfaces with outdated channel state information: Centralized vs. distributed deployments," *IEEE Transactions on Communications*, early access, Jan. 26, 2022, doi : 10.1109/TCOMM.2022.3146344.

[7] Y. Xu, H. Xie, Q. Wu, C. Huang, and C. Yuen, "Robust max-min energy efficiency for RIS-aided HetNets with distortion noises," *IEEE Transactions on Communications*, vol. 70, no. 2, pp. 1457–1471, 2022.

[8] J. Lyu and R. Zhang, "Spatial throughput characterization for intelligent reflecting surface aided multiuser system," *IEEE Wireless Communications Letters*, vol. 9, no. 6, pp. 834–838, 2020.

[9] L. Wei, C. Huang, G. C. Alexandropoulos, C. Yuen, Z. Zhang, and M. Debbah, "Channel estimation for RIS-empowered multi-user MISO wireless communications," *IEEE Transactions on Communications*, vol. 69, no. 6, pp. 4144–4157, 2021.

[10] Q.-U.-A. Nadeem, A. Zappone, and A. Chaaban, "Intelligent reflecting surface enabled random rotations scheme for the MISO broadcast channel," *IEEE Transactions on Wireless Communications*, vol. 20, no. 8, pp. 5226–5242, 2021.

[11] J. Hu, K. Yang, G. Wen, and L. Hanzo, "Integrated data and energy communication network: A comprehensive survey," *IEEE Communications Surveys Tutorials*, vol. 20, no. 4, pp. 3169–3219, 2018.

[12] D. Gunasinghe and G. A. A. Baduge, "Performance analysis of SWIPT for intelligent reflective surfaces for wireless communication," *IEEE Communications Letters*, vol. 25, no. 7, pp. 2201–2205, 2021.

[13] C. Pan, H. Ren, K. Wang, M. Elkashlan, A. Nallanathan, J. Wang, and L. Hanzo, "Intelligent reflecting surface aided MIMO broadcasting for simultaneous wireless information and power transfer," *IEEE Journal on Selected Areas in Communications*, vol. 38, no. 8, pp. 1719–1734, 2020.

[14] Y. Xu, Z. Gao, Z. Wang, C. Huang, Z. Yang, and C. Yuen, "RIS-enhanced WPCNs: Joint radio resource allocation and passive beamforming optimization," *IEEE Transactions on Vehicular Technology*, vol. 70, no. 8, pp. 7980–7991, 2021.

[15] Y. Xiao, P. D. Diamantoulakis, Z. Fang, L. Hao, Z. Ma, and G. K. Karagiannidis, "Cooperative hybrid VLC/RF systems with SLIPT," *IEEE Transactions on Communications*, vol. 69, no. 4, pp. 2532–2545, 2021.

[16] G. Pan, J. Ye, and Z. Ding, "Secure hybrid VLC/RF systems with light energy harvesting," *IEEE Transactions on Communications*, vol. 65, no. 10, pp. 4348–4359, 2017.

[17] P. Xu, G. Chen, G. Pan, and M. D. Renzo, "Ergodic secrecy rate of RIS-assisted communication systems in the presence of discrete phase shifts and multiple eavesdroppers," *IEEE Wireless Communications Letters*, vol. 10, no. 3, pp. 629–633, 2021.

[18] H. Ren, K. Wang, and C. Pan, "Intelligent reflecting surface-aided URLLC in a factory automation scenario," *IEEE Transactions on Communications*, vol. 70, no. 1, pp. 707–723, 2022.

[19] L. Yang, J. Yang, W. Xie, M. O. Hasna, T. Tsiftsis, and M. D. Renzo, "Secrecy performance analysis of RIS-aided wireless communication systems," *IEEE Transactions on Vehicular Technology*, vol. 69, no. 10, pp. 12 296–12 300, 2020.

[20] I. S. Gradshteyn and I. M. Ryzhik, *Table of Integrals, Series, and Products, 7th.* San Diego, CA: Academic Press, 2007.

[21] S. P. and M. R., *Spectral Analysis of Signals.* Upper Saddle River, NJ, USA: Prentice-Hall, 2005.

[22] F. E. Bouanani, S. Muhaidat, P. C. Sofotasios, O. A. Dobre, and O. S. Badarneh, "Performance analysis of intelligent reflecting surface aided wireless networks with wireless power transfer," *IEEE Communications Letters*, vol. 25, no. 3, pp. 793–797, 2021.

[23] Z. Li, W. Chen, Q. Wu, K. Wang, and J. Li, "Joint beamforming design and power splitting optimization in IRS-assisted SWIPT NOMA networks," *IEEE Transactions on Wireless Communications*, vol. 21, no. 3, pp. 2019–2033, 2022.

[24] T. Van Chien, L. T. Tu, S. Chatzinotas, and B. Ottersten, "Coverage probability and ergodic capacity of intelligent reflecting surface-enhanced communication systems," *IEEE Communications Letters*, vol. 25, no. 1, pp. 69–73, 2021.